Sustainable Food Technology

ROYAL SOCIETY OF CHEMISTRY

PAPER

View Article Online
View Journal

Cite this: DOI: 10.1039/d6fb00025h

Generating high-value porous materials from fruit and vegetable waste

Niveditha Asaithambi[a] and Ali Ubeyitogullari *[ab]

Fruit and vegetable waste is a global concern due to its significant environmental impact, economic loss, and implications for food security. In this study, fruit and vegetable waste was used as whole materials, avoiding extraction, to produce aerogels *via* supercritical carbon dioxide (SC-CO_2) drying for applications of dye removal. Aerogels were produced from banana peel (BPA), broccoli stem (BSA), cabbage leaves (CLA), imperfect carrot (ICA), and orange peel (OPA). The resulting aerogels exhibited low density (<1 g cm^{-3}), high porosity (>93%), and high surface areas (12–172 m^2 g^{-1}), with OPA showing the highest value at 172 m^2 g^{-1}. The CLA samples had the highest pore size (29 nm), contributing to their highest water absorption capacity of 95%. SEM images showed a promising porous structure and highlighted the fibrillar structure in OPA samples. The average methylene blue adsorption capacity was ~84%, except for OPA samples (53%). The methylene blue adsorption was driven by electrostatic interactions, which highly correlated with the pseudo-first order kinetic model (R^2 > 0.98). Overall, this study demonstrates that whole fruit and vegetable waste can be effectively converted into lightweight, highly porous aerogels with potential applications in biomedical and food fields, purification and filtration systems, and other functional materials sectors.

Received 21st January 2026
Accepted 18th April 2026

DOI: 10.1039/d6fb00025h

rsc.li/susfoodtech

Sustainability spotlight

This work addresses the global challenge of fruit and vegetable waste by valorizing the whole food residues into high-value, functional aerogels without extraction or chemical-intensive processes. Using SC-CO_2 as a sustainable green technique for drying, we process fruits and vegetable waste materials such as banana peels, broccoli stems, cabbage leaves, imperfect carrots, and orange peels into lightweight, highly porous aerogels for various applications, including wastewater treatment. This approach supports circular economy principles by reducing food waste, minimizing resource use, and creating sustainable materials for water purification and filtration. Moreover, the study contributes to the UN Sustainable Development Goals (SDG) of responsible production and consumption as well as safe water, sanitization, and hygiene by highlighting both waste reduction and sustainable water treatment solutions.

1 Introduction

Food waste represents a major global challenge in the food industry. Developing sustainable strategies to valorize these waste materials is crucial for promoting circular economy practices. According to the Food and Agriculture Organization of the United Nations (FAO), approximately 1.3 billion tons of food are wasted each year globally, resulting in an estimated monetary loss of about USD 936 billion, excluding the significant environmental and social costs borne by society as a whole.[1] The United Nations Sustainable Development Goal (SDG) Target 12.3 aims to reduce the global food loss and waste by 50% by 2030, through prevention, reduction, recycling, and reuse of food resources. Achieving this task requires the development of innovative technologies and processing strategies to support regenerative practices, conserve resources, and minimize greenhouse gas emissions, which have become a crucial focus in recent years.[2]

Among total food waste, approximately 16% is contributed by fruits and vegetables, which also account for about 6% of global greenhouse gas emissions.[3] The wide diversity of horticultural products makes them unique among food resources, offering numerous possibilities for value addition through innovative processing and utilization of their natural components. Most studies on fruit waste utilization focus on the recovery of bioactive compounds that exhibit antioxidant, antimicrobial, or health-promoting properties with potential applications in pharmaceuticals, packaging films, and functional food development.[4,5] However, the efficiency of bioactive compound extraction depends on several critical factors, including the source material, extraction technology, and processing methods, and still leaves behind a large fraction of food waste materials.[6] Therefore, an alternative strategy for food waste valorization involves converting it into high-value

[a]Department of Food Science, University of Arkansas, 2650 N. Young Ave., Room N205, Fayetteville, AR 72704, USA. E-mail: uali@uark.edu; Tel: +1 (479)-575-3183
[b]Department of Biological and Agricultural Engineering, University of Arkansas, Fayetteville, AR 72701, USA

aerogels through green, sustainable, and economically viable methods.[2]

Another major environmental concern is the organic dyes used in the paper and textile industries to enhance their aesthetic appeal and gloss, which are a major source of water pollution.[7] Their presence in wastewater poses serious environmental and health risks, making their removal a critical global concern. Although several remediation strategies have been developed, the elimination of dyes remains challenging due to their complex molecular structures, large size, and high chemical stability, particularly in the case of dyes such as methylene blue.[8,9]

Aerogels are porous materials characterized by high surface area (>100 $m^2 g^{-1}$), low density, excellent absorption capacity, and low thermal conductivity.[10] They are typically produced from organic or synthetic polymers by first forming a gel, followed by solvent exchange to remove the water, and finally drying *via* SC-CO_2. This results in a solid network of interconnected nanoparticles or polymer chains filled mostly with air.[11] Recent research has focused more on developing biobased aerogels that are environmentally friendly and economically viable. Some of the common biopolymers used in aerogel preparation include polysaccharides (*e.g.*, starch, pectin, alginate, chitosan, chitin, cellulose, and its derivatives) and, in some cases, proteins.[12–14] Recently, Possari, *et al.*[15] utilized biomass from the orange juice industry to produce biobased aerogels using citric acid hydrolysis. These biopolymer-derived aerogels, which rely on processing and extraction-based approaches, have found numerous applications, including use as an insulating material, adsorbents, biomedical applications, and active food packaging.[12,16]

Although aerogels have been successfully produced from natural biopolymers, the extraction process is often time-consuming and labor-intensive. Moreover, these aerogels often involve the use of hazardous chemicals during processing, which can pose environmental and health risks and limit their overall sustainability.[17–19] Therefore, developing simpler and more innovative methods for aerogel production is essential. In this study, for the first time, we report the direct conversion of fruit and vegetable waste into aerogels to understand their structural and functional characteristics for potential future applications. Previously, Gibowsky, *et al.*[2] utilized fresh fruits and vegetable tissues that were pulp removed or shredded, solvent-exchanged using ethanol, and then dried using SC-CO_2, to form porous aerogels. However, the biowaste as a whole was not utilized in previous studies. Therefore, aerogels derived from food waste not only address waste management concerns but also provide an eco-friendly and versatile platform for the efficient adsorption and removal of organic dyes from wastewater. Here, we employ SC-CO_2 technology, a widely used, green, cost-effective, and unique technique that is Generally Recognized as Safe (GRAS) to produce aerogels. The technology has been advantageous in producing aerogels with a high surface area. In our previous study,[14] we found that the SC-CO_2-dried starch beads showed a significantly higher surface area (175 $m^2 g^{-1}$) than the freeze-dried ones (<1 $m^2 g^{-1}$).

Therefore, in this study, we investigated the direct formation of food waste-derived aerogels from various fruit and vegetable sources (*i.e.*, banana peel, broccoli stem, cabbage leaves, imperfect carrot, and orange peel) using SC-CO_2 drying. These fruit and vegetable waste samples were selected due to their generation in large quantities as well as their potential to form a porous structure.[20,21] The samples were characterized for their physicochemical and structural properties for their potential applications in the removal of dyes to prevent environmental pollution.

2 Experimental section

2.1. Materials

The fruit and vegetable samples, including navel orange peels, imperfect carrots, broccoli stems, cabbage leaves, and banana peels, were obtained from a local store/farm. The ethanol utilized for solvent exchange was purchased from Decan Labs, Inc. (Koptec, Pure Ethanol 200 Proof, PA, USA). The liquid CO_2 (99.99% purity) for the SC-CO_2 system was procured from Airgas, Inc. (AR, USA).

2.2. Aerogel formation

For aerogel preparation, all materials were cut into small pieces (~1–5 cm) and weighed before the solvent exchange process. Next, the prepared samples were solvent exchanged by sequential immersion in ethanol/water solutions of 30%, 50%, 70% and 100% ethanol, each for 1 h, followed by immersion in 100% ethanol for 24 h. Later, the samples were dried using a lab-scale SC-CO_2 system (SFT-120, Supercritical Fluid Technologies Inc., DE, USA) at 10 MPa and 40 °C for 4 h, with a CO_2 flow rate of 1.0 L min^{-1} (measured under ambient conditions of 23 °C and 0.1 MPa).[13] The resulting aerogels were then collected and stored at room temperature (23 °C) in airtight containers until further analysis.

2.3. Moisture content

The moisture contents of fresh fruit and vegetable samples were determined based on our previous study.[22] The samples were dried in a conventional oven at 105 °C for 12 h, and the moisture content (%, wet basis) was calculated based on the weight loss observed after drying.

2.4. Ash content

The ash contents of aerogels were determined using the method followed by Liu,[23] where the aerogel samples were heated in a muffle furnace (Barnstead Thermolyne 1400 Furnace, NY, USA) at 600 °C and left overnight. The ash contents of the samples were obtained by calculating the total ash content as % sample mass (in dry basis).

2.5. Density, porosity, and shrinkage

The bulk density of the samples was measured using the weight-to-volume ratio by filling a known weight of the sample into a measuring cylinder and recording its corresponding volume. The true density was measured using a gas pycnometer

(AccuPyc II 340, Micromeritics, GA, USA) at room temperature (23 °C) in a 10 cm^3 cell, with purge and cycle fill pressures maintained at 19.5 psig. The porosity was calculated from bulk and true density using the following eqn (1):

$$\text{Porosity}(\%) = \left(1 - \frac{\text{bulk density}}{\text{true density}}\right) \times 100 \quad (1)$$

2.6. Surface area, pore size, and pore volume

The surface area, pore size, and volume of the aerogel were analyzed using a low-temperature nitrogen adsorption–desorption (TriStar II Plus, Micromeritics Instrument Corporation, GA, USA). Approximately 0.1–0.3 g of each aerogel sample was placed in the sample tubes and degassed at 75 °C for 24 h.[14] The nitrogen sorption measurements were performed at −196 °C. The specific surface area was calculated using the multipoint Brunauer–Emmett–Teller (BET) method within a relative pressure range (p/p_0) of 0.05–0.3, whereas the Barrett–Joyner–Halenda (BJH) method was used to determine pore size and volume at relative pressures above 0.35.

2.7. Scanning electron microscopy

The microstructural images of the aerogels were taken following the method outlined by Sadaf, *et al.*,[22] using a FEI Nova Nanolab 200 Dual Beam system (FEI Company, OR, USA), which is equipped with a 30 kV FIB column and 30 kV SEM FEG column. Prior to imaging, the aerogel samples were coated in a gold layer at a deposition rate of 25 nm min^{-1} using an EMITECH SC7620 Sputter Coater (MA, USA). The SEM analysis was performed at 15 kV and 15 mA in low-vacuum mode, with a working distance of 5 mm. The SEM images were captured at magnifications of 500× and 5000×.

2.8. X-ray diffraction (XRD)

The XRD pattern of aerogels was analyzed using a high-resolution X-ray diffractometer (Philips, Almelo, Netherlands), following the method of Sadaf, *et al.*[22] The XRD measurements were conducted at 45 kV and 40 mA, scanning over a 2θ range of 5° to 60° with a step size of 0.02° and a scan speed of 0.0167° s^{-1}.

2.9. Fourier transform infrared spectroscopy

FTIR spectra of aerogel samples were recorded using a Shimadzu IRAffinity-1S spectrometer equipped with a Quest ATR accessory. The spectral data were collected from 400 to 4000 cm^{-1} with a resolution of 8 cm^{-1} over 64 scans.[24]

2.10. Water absorption

The water absorption capacity of aerogels was evaluated by following the method of Silva, *et al.*[25] The samples were weighed before and after water immersion (1 : 50, w/v) for about 24 h. The water absorption capacity was determined using eqn (2):

$$\text{Water absoprtion capacity}(\%) = \left(\frac{\text{SW} - \text{DW}}{\text{DW}}\right) \times 100 \quad (2)$$

where SW and DW are the swollen and dry weight of the aerogel, respectively.

2.11. Methylene blue adsorption capacity

Methylene blue adsorption experiments were conducted based on the method followed by Nguyen, *et al.*[26] with minor modifications. Aerogel samples (0.05 g) were added to 50 mL methylene blue solution (15 mg mL^{-1}, pH 7) and maintained at 30 °C in a shaker bath operating at 50 rpm. Aliquots of 2.5 mL were withdrawn at required time intervals (until equilibrium) and their absorbance measured at 665 nm using a spectrophotometer (Milton Roy Spectronic 1201 spectrophotometer, PA, USA). The adsorption capacity at time (Q_t), the equilibrium adsorption capacity (Q_e), and methylene blue removal efficiency (R_e), were calculated using the following eqn (3) and (4):

$$Q_t(\text{mg g}^{-1}) = \frac{(C_0 - C_t) \times V}{m} \quad (3)$$

$$Q_e(\text{mg g}^{-1}) = \frac{(C_0 - C_e) \times V}{m} \quad (4)$$

$$R_e(\%) = \frac{(C_0 - C_e)}{C_0} \times 100 \quad (5)$$

where C_0, C_t, and C_e (mg L^{-1}) represent initial, time-dependent (min), and equilibrium concentration of methylene blue, respectively. V (L) is the volume of the methylene blue solution, and m (g) is the mass of the adsorbent.

2.12. Adsorption kinetics

To further understand the adsorption mechanism, the adsorption kinetics prediction was evaluated using pseudo-first-order and second-order models expressed by eqn (6) and (7):[27]

$$\ln(q_e - q_t) = \ln q_e - k_1 \times t \quad (6)$$

$$\frac{t}{q_t} = \frac{1}{k_2 \times {q_e}^2} + \frac{1}{q_e} \times t \quad (7)$$

where q_e (mg g^{-1}) represents the amount of adsorbed methylene blue at equilibrium, q_t (mg g^{-1}) represents the amount of methylene blue adsorbed at time t, and k_1 (min^{-1}) and k_2 (g (mg min)$^{-1}$) are the pseudo-first-order and second-order rate constants, respectively.

The initial adsorption rate ν_0 (mg (g min)$^{-1}$) at time 0 could be calculated by the following eqn (8):

$$\nu_0 = k_2 \times {q_e}^2 \quad (8)$$

2.13. Statistical analysis

All measurements were taken in triplicate, and the results are presented as mean ± standard deviation. Statistical analysis was performed using ANOVA in JMP Pro (Version 17.0.0, SAS Institute, NC, USA), followed by Tukey's test with a significance of $p < 0.05$.

3 Results and discussion

3.1. Moisture content

The moisture content of the fresh samples was determined as 89.38 ± 0.10%, 94.10 ± 0.36%, 93.27 ± 0.17%, 89.43 ± 0.68%, and 74.73 ± 0.04% w.b for BPA, BSA, CLA, ICA, and OPA, respectively. The OPA had the lowest, and the BSA had the highest moisture content. The differences in moisture content among the fruit and vegetable waste samples can be attributed to their inherent tissue structure and composition.[28] Moreover, the primary cell wall and middle lamella are most responsible for the texture and structure of fruits and vegetables.[29] Most of the dry mass of the banana peel comes from its fiber content, made up of cellulose (7.6–9.6%), hemicellulose (10–21%), and lignin (6–12%).[30] In case of orange peels, the fibers include cellulose (22%), pectin (25%), and hemicellulose (11%) based on the percentage of whole peels.[31–33] The other fruit and vegetable waste, including carrots, cabbage leaves, and broccoli stems, had fiber content less than 3%.[34] Within which the carrots had a water-insoluble polysaccharide content including cellulose, hemicellulose, and lignin of 71.7%, 13.0%, and15.2%, respectively.[35] In broccoli stems, cellulose, hemicellulose, and pectin accounted for 18.5 ± 2.1%, 24.1 ± 0.3%, and 57.8 ± 2.8%, respectively,[36] whereas in cabbage leaves, cellulose, hemicellulose, and lignin were the major components as 9.07 ± 3.67%, 1.48 ± 0.95%, and 9.82 ± 3.56%, respectively.[37] The composition of the fruits and waste vegetable samples largely influenced the surface area of aerogels.

3.2. Ash content

The BPA (8.16 ± 0.45%) had the highest ash content, while the OPA (3.08 ± 0.70%) had the lowest (Table 1). The variation in ash content represents the difference in mineral content in the fruit and vegetable waste samples. Similar results were reported by Zhang, *et al.*,[38] where the banana peels had the highest ash content, while the orange peels had the lowest. The presence of ash content can be correlated to the thermal resistance of aerogels. For example, in a study by Khodavandegar, *et al.*[39] investigating chitosan–lignin aerogels, the authors reported that the composite with higher ash content (reflecting more inorganic or char-forming content) produced higher char yield and better thermal resistance during decomposition.

3.3. Density and porosity

The SC-CO_2-dried aerogels from different fruit and vegetable waste sources are presented in Fig. 1. The true density almost remained the same (~1.45 ± 0.01 g cm^{-3}) across all samples except for cabbage and carrot, which had slightly higher density values (~1.49 g cm^{-3}). The variation in true density may result from changes in molecular or structural arrangements, which may occur during a second-order phase transition influenced by its thermal history.[40] The bulk density of the aerogels (~0.1 g cm^{-3}) showed minimal variation across samples. In contrast, porosity values varied significantly ($p < 0.05$). The porosity as high as above 90% is a characteristic of aerogels for its utilization in food applications, including thermal insulations in packaging, carriers for flavors, nutrients, fat and sugar replacers, and texture enhancers. Their high porosity, low density, and varied surface properties make them ideal for encapsulation and controlled release of bioactive compounds.[41] Similar to these results, Gibowsky, *et al.*,[2] reported high-porosity values above 97% for food-waste aerogels derived from natural fruit and vegetable tissues, demonstrating their strong potential for application in oleogelation. The study assessed 20 different tissues, including apple, pear, plum, banana peel, orange peel, orange pulp, kiwi, radish, carrot, bell pepper, cucumber, tomato, onion, nectarine, strawberry, mushroom, and others. The study utilized fresh tissues that were washed, shredded, or pulp removed, solvent-exchanged using ethanol, and then dried using SC-CO_2, converting the native cellular structure to porous aerogels. The resulting aerogels were then categorized into three structural groups based on their pore-size distributions including category 1 with primarily small mesopores (pore diameter ≤ 6.5 nm), category 2 with mixed mesopore populations (with pore diameters small (≤6.5 nm), mid (≈6.5–10 nm), and larger mesopores (≈10–50 nm)), and category 3 dominated by larger mesopores (pore diameter 10–50 nm). Irrespective of the category, all samples had a high porosity above 97%.

3.4. Surface area, pore size, and pore volume

The OPA samples had the highest surface area (171.78 ± 6.67 m^2 g^{-1}), followed by BPA (57.37 ± 4.64 m^2 g^{-1}), ICA (55.35 ± 12.24 m^2 g^{-1}), BSA (23.50 ± 3.26 m^2 g^{-1}), and CLA (12.21 ± 3.27 m^2 g^{-1}) (Table 1). The pore size volume was also high in the case

Table 1 Ash content, density, porosity, surface area, pore volume, pore size, and water absorption capacity of fruit and vegetable waste aerogels[a]

Aerogel sample	BPA	BSA	CLA	ICA	OPA
Ash content (%)	8.16 ± 0.45^{a}	7.26 ± 0.41^{ab}	5.25 ± 1.28^{bc}	6.36 ± 0.03^{ab}	3.08 ± 0.70^{c}
True density (g cm^{-3})	1.46 ± 0.01^{b}	1.46 ± 0.01^{b}	1.50 ± 0.004^{a}	1.49 ± 0.01^{a}	1.44 ± 0.01^{b}
Bulk density (g cm^{-3})	0.08 ± 0.01^{a}	0.08 ± 0.02^{a}	0.11 ± 0.06^{a}	0.10 ± 0.01^{a}	0.10 ± 0.0001^{a}
Porosity (%)	94.69 ± 0.02^{a}	94.57 ± 0.02^{b}	92.53 ± 0.02^{e}	93.22 ± 0.03^{d}	93.41 ± 0.03^{c}
BET surface area (m^2 g^{-1})	57.37 ± 4.64^{b}	23.50 ± 3.26^{c}	12.21 ± 3.27^{c}	55.35 ± 12.24^{b}	171.78 ± 6.67^{a}
Pore volume (cm^3 g^{-1})	0.21 ± 0.002^{b}	0.11 ± 0.01^{cd}	0.08 ± 0.01^{d}	0.15 ± 0.03^{c}	0.45 ± 0.01^{a}
Pore size (nm)	14.35 ± 1.52^{b}	19.19 ± 0.60^{ab}	28.79 ± 6.78^{a}	9.83 ± 0.46^{b}	9.17 ± 0.23^{b}
Water absorption capacity (%)	1127.7 ± 17.39^{c}	2006.8 ± 3.68^{a}	2038.1 ± 0.42^{a}	1600 ± 118.79^{b}	674.2 ± 50.91^{d}

[a] Means ± standard deviation bars that do not share a common letter within each property (row) are significantly different ($p < 0.05$). BPA: banana peel aerogel; BSA: broccoli stem aerogel; CLA: cabbage leaf aerogel; ICA: imperfect carrot aerogel, and OPA: orange peel aerogel.

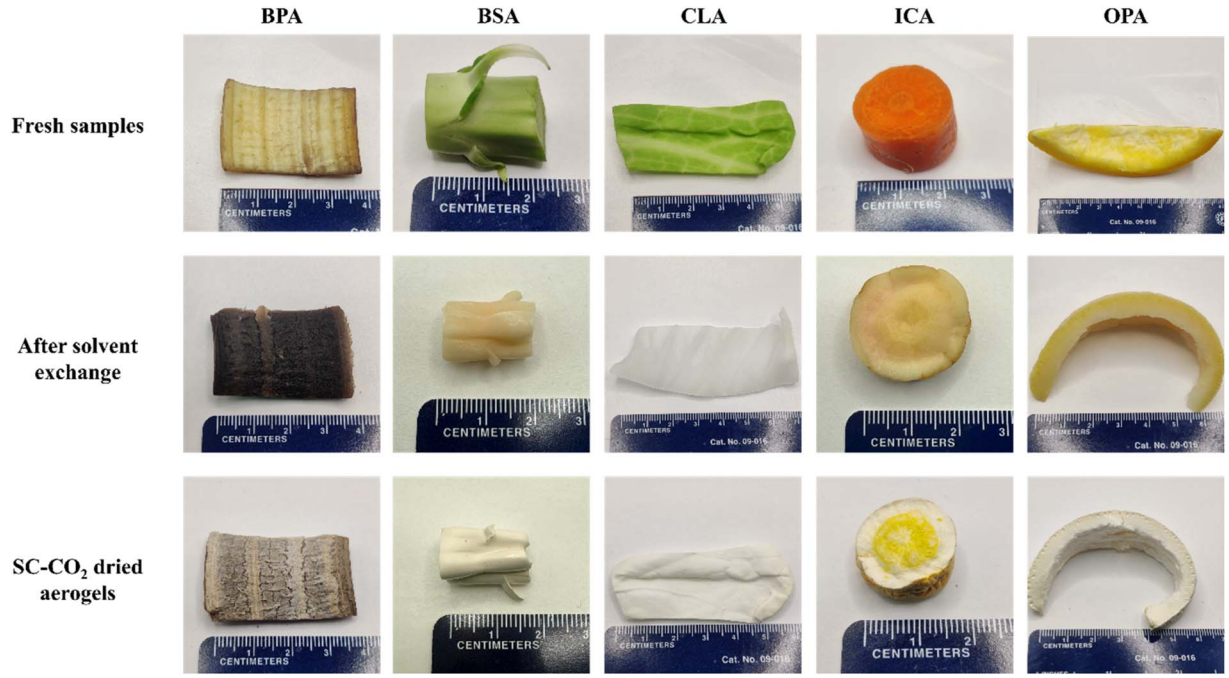

Fig. 1 Photographs of the aerogel at different stages of processing: fresh, solvent exchange, and dried stages. BPA: banana peel aerogel; BSA: broccoli stem aerogel; CLA: cabbage leaf aerogel; ICA: imperfect carrot aerogel, and OPA: orange peel aerogel.

of OPA (0.45 ± 0.01 cm^3 g^{-1}). The higher pore size and surface area of the OPA can be attributed to the presence of fibrils within the microstructure of OPA samples. Moreover, the high surface area of OPA can also be attributed to its composition, which contains a high amount of pectin and cellulose.[15] The presence of cellulose with insoluble fibers contributes to the development of a large surface area.[42] Following OPA, the BPA samples had a high surface area, likely due to the presence of similar constituents such as cellulose and pectin that contribute to pore formation and fibrous network; however, the surface area of BPA was lower than that of the OPA, attributing to varied cellulose content.[43,44]

Next to BPA (57.37 ± 4.64 m^2 g^{-1}), ICA (55.35 ± 12.24 m^2 g^{-1}) had a higher surface area, which can be attributed to the presence of higher cellulose content in carrots. Shih, *et al.*[45] produced bio-aerogels from cellulose nanofibers extracted from carrot pulp and reported a porous structure with a large surface area, demonstrating excellent swelling capacity. The high surface area of ICA can also be attributed to the presence of soluble and insoluble fibers present in carrot samples.[46] The presence of soluble fibers can enhance the porosity as it attracts water to form a gel matrix, while the insoluble fibers also form a matrix; however, it does not expand in water.[47] The BSA and CLA samples had the lowest surface area of 23.50 ± 3.26 m^2 g^{-1} and 12.21 ± 3.27 m^2 g^{-1}, respectively. It can be due to the significantly higher water content present in these samples when compared to other fruit and vegetable waste samples. Dourbash, *et al.*[48] concluded that higher initial water content decreased the surface area and porosity of silica aerogel samples. When the water content is lower, the surface is more likely to undergo complete chemical modification, leading to the "spring-back effect", which consequently reduces the volume shrinkage.[49,50] Moreover, the pore size of the BSA and CLA was also large, demonstrating the lower surface area. This is because a material with larger pores will have fewer pores in a given volume compared to a material with smaller pores, and the total surface area is the sum of the area of all the pores. A material with many smaller pores will have a higher total internal surface area.[51]

3.5. Morphology

The SEM images of the aerogels (Fig. 2) revealed a well-defined porous structure with intact hexagonal cell arrangements, confirming that SC-CO_2 drying effectively preserved the microstructure of all the samples. Among the samples, CLA samples had noticeably larger pores, whereas OPA, BPA, and ICA depicted smaller macropores. The larger pore size observed in CLA can be useful for adsorption, especially in biomedical applications,[16] further supported by the relatively high surface area of these samples. At higher magnification, OPA and BPA samples revealed fine fibrillar networks, with OPA showing more extensive fibrillation, which contributes to the higher surface area of these samples. The high surface area of aerogels enables a wide range of applications, including adsorption and filtration, drug delivery, and other biomedical applications, as well as thermal insulation.[52]

3.6. Crystallinity

The aerogel samples exhibited an amorphous nature in general, with varied crystallinity among different aerogel samples (Fig. 3A). The OPA and BPA samples exhibited sharp diffraction peaks around 15°, 17°, 22°, and 35° 2θ angle, indicating the presence of crystalline cellulose components.[53] The observed

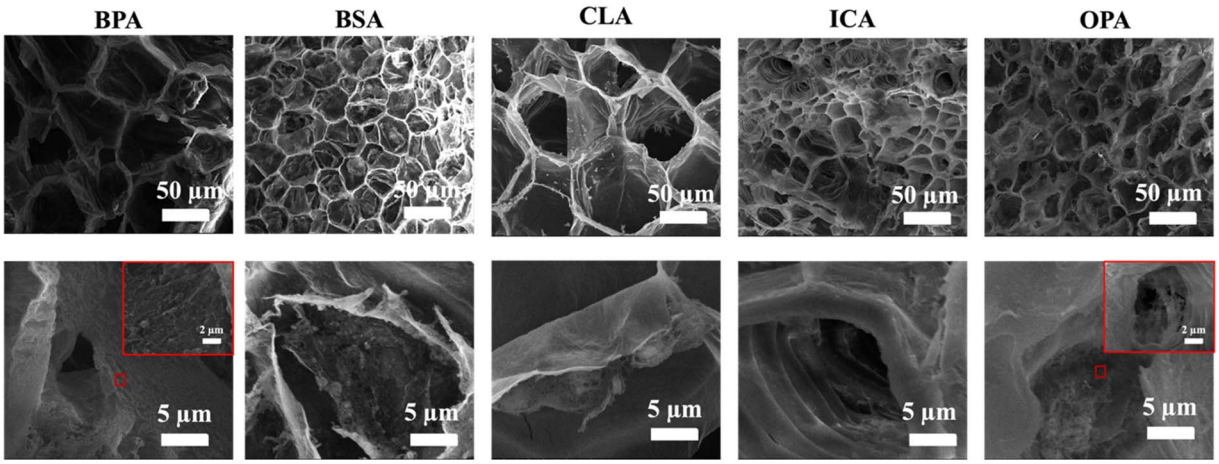

Fig. 2 SEM images of fruits and vegetable waste aerogels taken at 500× and 5000×. BPA: banana peel aerogel; BSA: broccoli stem aerogel; CLA: cabbage leaf aerogel; ICA: imperfect carrot aerogel, and OPA: orange peel aerogel.

crystallinity can be attributed to the hydrogen bonding interactions and van der Waals forces between adjacent molecules, whereas the remaining lignin and cellulose components exhibited a more amorphous nature.[54] The ICA and BSA had sharp peaks near 21.5° 2θ angle, indicating the presence of pectin.[55,56] The pectin typically exists in an amorphous or semi-crystalline state, due to hydrogen bonding among hydroxyl groups within the polysaccharide chain.[57] Even though the BSA and ICA samples displayed the presence of ordered structure, it was less pronounced compared to the peel samples, OPA and BPA. In contrast, the CLA samples did not display a distinct, sharp peak but rather a broader peak near 21.5°, which could represent lignin present in the samples, which also presented a broad amorphous peak centered around 21.5°.[58]

3.7. Chemical interaction

The FTIR spectra provided information on the functional groups present in the aerogels (Fig. 3B), where typical lignocellulosic material characteristics were observed. All the samples had a broad peak near 3100–3600 cm^{-1}, representing the –OH stretching vibration. Among all the samples, CLA had a broader peak, representing a strong hydrogen bonding interaction. In addition, the aerogels exhibited peaks near 2920 and 2850 cm^{-1}, corresponding to the asymmetric and symmetric stretching vibrations of C–H bonds.[59] The peaks at 2850 cm^{-1} were more visible in the CLA, possibly due to a higher content of aliphatic C–H groups derived from lipids or cuticular wax components present in cabbage leaves, which remained during aerogel formation.[60] Further, the peak around 1735 cm^{-1} corresponded to the stretching vibration of the carboxyl functional group C=O ester bond. In plant cells, this absorption is mainly attributed to the esterified carboxyl groups in pectin (methyl esters of galacturonic acid) or other ester-containing components. The FTIR spectra showed that the OPA and CLA samples exhibited stronger peaks near 1735 cm^{-1}, suggesting a higher content of esterified compounds, whereas the BSA, ICA, and BPA samples displayed much weaker peaks,

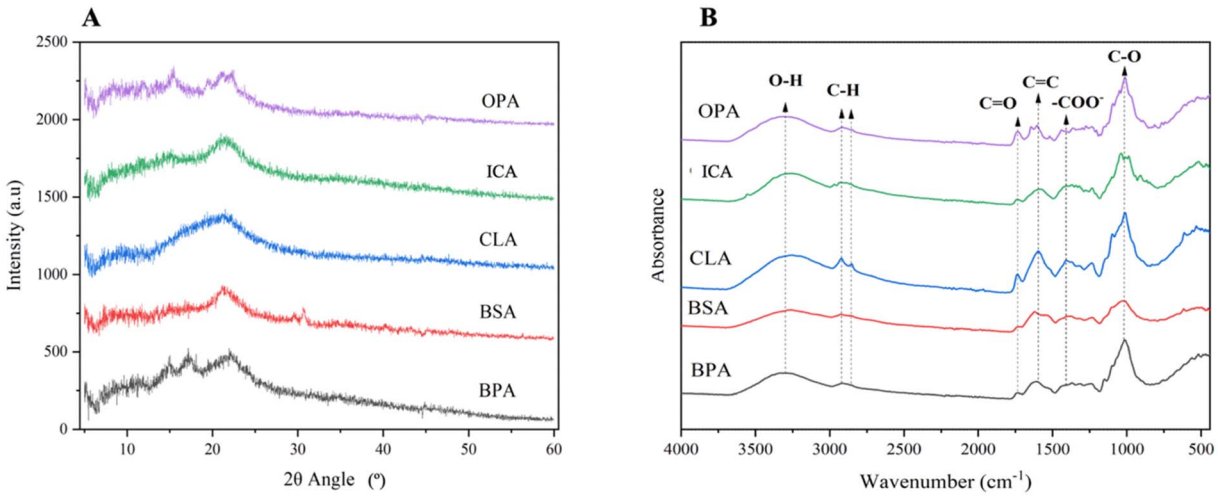

Fig. 3 The (A) XRD patterns and (B) FTIR spectrum of fruits and vegetable waste aerogels. BPA: banana peel aerogel; BSA: broccoli stem aerogel; CLA: cabbage leaf aerogel; ICA: imperfect carrot aerogel, and OPA: orange peel aerogel.

indicating a lower degree or possible absence of these ester groups.[58,61]

The region from 1600 to 1321 cm^{-1} is dominated by carboxylate ($–COO^-$) vibrations. The band near 1600–1585 cm^{-1} corresponded to the aromatic rings of C=C stretching, while the peaks at 1415 and 1315 cm^{-1} were due to symmetric $–COO^-$ stretching and C–O (~1050 cm^{-1}) deformation vibrations.[53] These features indicate the presence of carboxylate-containing polysaccharides, such as pectin and hemicellulose, which were more prominent in CLA, BSA, and ICA, reflecting their amorphous nature. In contrast, BPA and OPA, which contained higher cellulose content, exhibited slightly weaker and narrower peaks, consistent with increased structural ordering.[62]

3.8. Water absorption capacity

All the aerogel samples had a high-water absorption capacity, exceeding 670% (Table 1). Among them, CLA and BSA showed the highest absorption (~2000%), which can be attributed to their larger pore sizes facilitating greater water absorption. Yin, *et al.*[63] reported similar trends in Balsa wood aerogels, where larger pore sizes enabled faster absorption rate and greater absorption capacity. The ICA samples also demonstrated high water absorption (1600%), likely due to their porosity and their high ratio of soluble fibers, which enhance water retention by forming a gel network. This is consistent with the findings of Shih, *et al.*,[45] who reported high water absorption up to 1100% in carrot pulp aerogels. In contrast, the peel samples, BPA, and OPA had slightly lower water absorption capacity of 1127.7 ± 17.39% and 674.2 ± 50.91% than non-peel samples, including BSA (2006.8 ± 3.68%), CLA (2038.1 ± 0.42%), and ICA (1600 ± 118.79%), respectively. This can be attributed to their higher content of insoluble fibers, which limit water uptake.[64] These results are in agreement with earlier studies as reported by Wanlapa, *et al.*[65] Water absorption capacity can play important roles in food applications like active and intelligent food packaging, moisture control to extend shelf life, and absorbent pads for exudate management in fresh products. It can also be valuable in other applications, including atmospheric water harvesting and environmental cleanup, like water purification and separation for their high porosity, large surface area, and tunable hydrophilicity.[66,67]

3.9. Methylene blue adsorption capacity

The methylene blue adsorption capacity of aerogel samples is represented in Fig. 4. The methylene blue removal efficiency of BPA, BSA, CLA, ICA, and OPA was 87.99 ± 0.10%, 80.77 ± 0.16%, 78.59 ± 0.10%, 87.99 ± 0.38%, and 53.49 ± 0.32%, respectively. The removal efficiency of the OPA was the lowest when compared to other samples, which can be directly correlated to the microstructure of OPA, providing lower water and dye adsorption capacity. Despite the highest BET specific surface area of OPA, it showed lower methylene blue adsorption capacity compared to all samples. The adsorption performance is strongly influenced by pore size distribution and surface chemistry. In the OPA, a significant fraction of the surface area is likely associated with micropores (as indicated in SEM) that are not accessible to the relatively large methylene blue molecules, thereby limiting effective adsorption. Michael Igolima, *et al.*[68] also reported lower adsorption capacity of raw orange peels when compared to physically modified orange peels,

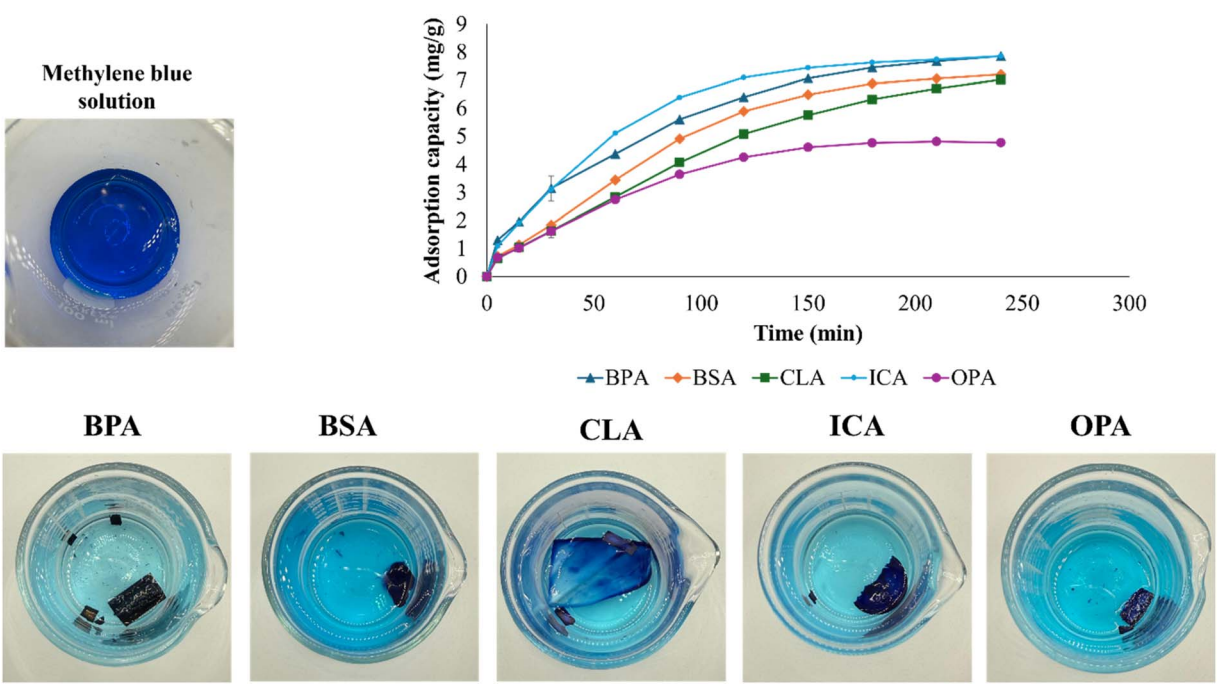

Fig. 4 Methylene blue adsorption capacity of aerogels. BPA: banana peel aerogel; BSA: broccoli stem aerogel; CLA: cabbage leaf aerogel; ICA: imperfect carrot aerogel, and OPA: orange peel aerogel.

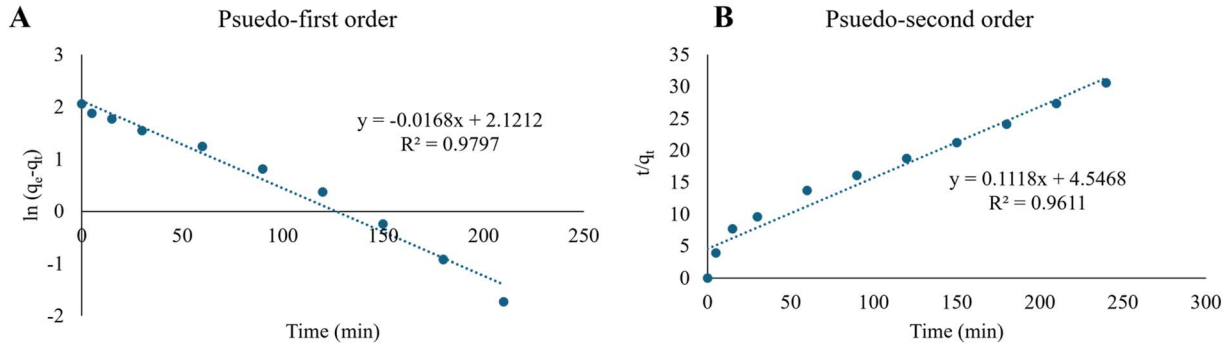

Fig. 5 Adsorption kinetics of methylene blue adsorption for (A) pseudo-first order model and (B) pseudo-second order model for BPA (banana peel aerogel).

which have increased the porous structure for the adsorption of contaminants. In accordance with this, the BPA and ICA, having moderate surface area with mesopores, had the highest methylene blue adsorption. Similar observations were concluded by Zhou, *et al.*,[69] where ultra-high surface area mesoporous carbon facilitated faster and more effective adsorption for bulk molecules like methyl blue compared to larger mesopores and microporous materials. In the case of BSA and CLA, the SEM morphology shows a large pore size, resulting in reduced methylene blue adsorption than ICA and BPA.

3.10. Adsorption kinetics

The value of adsorption kinetic parameters was assessed from the plots of pseudo-first order, and pseudo-second order linear plots (Fig. 5). These models help in predicting the equilibrium adsorption kinetics and identify the surface adsorption mechanism of methylene blue on aerogels.[70] In the initial stages of adsorption, till 120 min, there was an increase in adsorption capacity, which is 80% of the adsorption capacity, and later became constant. Methylene blue, being a cationic dye in aqueous solution, interacts electrostatically with adsorption sites such as –OH and –COOH functional groups present on the surfaces of aerogels in the adsorbent. Due to the availability of more active sites for methylene blue adsorption, the initial adsorption rate is higher; however, as time progresses, these free active sites diminish, resulting in a decreased adsorption rate.[71] The adsorption of methylene blue is governed by multiple interaction mechanisms, including π–π interactions, hydrogen bonding, surface complexation, electrostatic interactions, ion exchange processes, and van der Waals forces.[72] While electrostatic attraction between the cationic dye and negatively charged surface groups is a probable pathway for fruits and vegetable waste, other interactions also play significant roles.[73] The presence of hydroxyl, and carboxyl groups (as evidenced by FTIR analysis) facilitates adsorption through hydrogen bonding and surface interactions. In addition, π–π interactions between the aromatic structure of methylene blue and lignin-derived components of the fruits and vegetable waste may also contribute to adsorption.[74] Moreover, the highly porous structure of the aerogels further facilitates pore-filling and physical adsorption. Table 2 presents the kinetic model parameters calculated from the pseudo-first-order and second-order models (Fig. 5). From Table 2, it can be observed that the correlation coefficients (R^2) for all the aerogels were higher for the pseudo-first-order than the second-order kinetic curve, except for OPA, indicating that the adsorption involved chemical reactions (or chemisorption) in addition to physisorption.[75] The pseudo-second-order kinetic behavior suggests that the adsorption process is governed by interactions between the adsorbate and available active sites on the adsorbent surface. In OPA, this behavior can arise from the presence of abundant functional groups (*e.g.*, hydroxyl and carboxyl groups), which facilitate multiple interaction mechanisms including hydrogen bonding, electrostatic attraction, and surface complexation. However, it is important to note that pseudo-second-order kinetics does not exclusively confirm chemisorption but rather indicates that the adsorption rate is controlled by the availability and reactivity of surface sites.[76] Despite exhibiting the highest BET surface area, the adsorption rate was low, due to enhanced interaction of the abundant functional group with the cationic methylene blue dye, leading to surface-controlled adsorption consistent with pseudo-second-order kinetics.[77] Furthermore, the porous structure may introduce diffusion limitations, particularly within smaller pores, which further reduces the overall adsorption rate. Khumalo, *et al.*[76] explained that adsorption performance is governed more by functional group availability and pore accessibility than by surface area

Table 2 Kinetic parameters of pseudo-first-order kinetics and pseudo-second-order kinetics of methylene blue adsorption of aerogels

Kinetic parameters	BPA	BSA	CLA	ICA	OPA
Pseudo first-order kinetics					
q_e (mg g^{-1})	8.34	8.68	8.05	8.24	7.42
k_1 (min^{-1})	0.0168	0.0176	0.0136	0.02	0.0292
R^2	0.9797	0.9768	0.9646	0.9982	0.8619
Pseudo-second order kinetics					
q_e (mg g^{-1})	8.95	9.50	9.29	9.12	5.84
k_2 (g (mg min)$^{-1}$)	0.0027	0.0014	0.0012	0.0029	0.0035
R^2	0.9611	0.87	0.828	0.9693	0.9423
ν_0 (mg (g min)$^{-1}$)	0.22	0.12	0.10	0.24	0.12

alone, with the carboxymethyl cellulose-based silica aerogel providing more accessible binding sites and better diffusion pathways for methylene blue despite its lower BET surface area. For other food waste aerogels, the results identified that the pseudo-first-order kinetic model was more appropriate for describing the adsorption kinetics, favoring the surface area results. These results are consistent with previous studies, which reported that the methylene blue adsorption behavior of chitosan aerogels was better described by the pseudo-first-order model than by the pseudo-second-order model.[78] Moreover, the predicted q_e and v_0 were almost equivalent to the experimental results, confirming the suitability of the proposed model for describing methylene blue adsorption of food waste aerogels.

4 Conclusions

Nearly one-third of the world's food is lost, with fruits and vegetables being the most wasted despite their nutritional value. Producing aerogels from fruit and vegetable waste provides an effective upcycling route to convert this biomass into high-value materials. In this study, aerogels were prepared from BPA, BSA, CLA, ICA, and OPA. All aerogels exhibited highly porous structures, with densities below 0.1 g cm^{-3}, porosities above 93%, and high surface areas (12–172 m^2 g^{-1}). The peel samples showed the highest BET surface areas, reaching ~172 m^2 g^{-1} for OPA and ~57 m^2 g^{-1} for BPA. The pore size results revealed that CLA samples exhibited the largest pores, with an average BJH pore size of ~29 nm, which contributed to their highest water absorption capacity of 2000%. Crystallinity analysis indicated that the aerogels were predominantly amorphous, although OPA and BPA displayed relatively higher crystalline features, likely due to the presence of a cellulosic structure. FTIR spectra confirmed the presence of pectin, cellulose, and hemicellulose in all samples, with variations among the different fruit and vegetable sources. The methylene blue adsorption capacity was largely driven by electrostatic interaction, with an average adsorption capacity of ~84% except for OPA (53%). The pseudo-first order kinetics model better predicted the methylene blue adsorption kinetics compared to the pseudo-second order model, with $R^2 > 0.98$. Overall, this study demonstrates that fruit and vegetable waste can be effectively used as whole materials for aerogel production. This work minimizes the pretreatments needed to create biopolymer-based aerogels.

Author contributions

Niveditha Asaithambi: methodology, validation, formal analysis, writing – original draft, visualization. Ali Ubeyitogullari: conceptualization, methodology, supervision, validation, writing – review & editing, project administration, funding acquisition, resources.

Conflicts of interest

There are no conflicts of interest to declare.

Data availability

The data supporting this article have been included as part of the current article.

Acknowledgements

This project was supported, at least in part, by the USDA National Institute of Food and Agriculture, Multistate Project NC1023, Accession number 1025907, AFRI award no: 2023-67022-40164, and EGP 2024-70410-43765.

References

1 FAO, *Food Wastage Footprint Full-cost Accounting*, Final Report, 9251085129, Food & Agriculture Organization of the UN (FAO), Rome, Italy, 2014.
2 L. Gibowsky, L. De Berardinis, S. Plazzotta, E. Manke, I. Jung, D. A. Méndez, F. Heidorn, G. Liese, J. Husung, A. Liese, P. Gurikov, I. Smirnova, L. Manzocco and B. Schroeter, *Green Chem.*, 2025, **27**, 4713–4731, DOI: 10.1039/d4gc05703a.
3 L. Cassani and A. Gomez-Zavaglia, *Front. Nutr.*, 2022, **9**, 829061, DOI: 10.3389/fnut.2022.829061.
4 A. Niveditha, D. V. Chidanand and C. K. Sunil, *Meas. Food*, 2023, **12**, 100114, DOI: 10.1016/j.meafoo.2023.100114.
5 R. Karmakar, S. Aggarwal, D. Kathuria, N. Singh, V. Tripathi, P. K. Sharma, D. Mitra, S. Kumar and S. Bhattacharya, *Food Biosci.*, 2025, **69**, 106833, DOI: 10.1016/j.fbio.2025.106833.
6 A. A. Zaky, D. Witrowa-Rajchert and M. Nowacka, *Food Saf. Health*, 2025, **3**, 315–333, DOI: 10.1002/fsh3.70012.
7 W. A. El-Fattah, A. Guesmi, N. Ben Hamadi, M. G. El-Desouky and A. Shahat, *Colloids Surf., A*, 2024, **681**, 132729, DOI: 10.1016/j.colsurfa.2023.132729.
8 N. Saad, M. Al-Mawla, E. Moubarak, M. Al-Ghoul and H. El-Rassy, *RSC Adv.*, 2015, **5**, 6111–6122, DOI: 10.1039/c4ra15504a.
9 M. G. El-Desouky, M. A. G. Khalil, M. A. M. El-Afify, A. A. El-Bindary and M. A. El-Bindary, *Desalination Water Treat.*, 2022, **280**, 89–127, DOI: 10.5004/dwt.2022.29029.
10 A. Ubeyitogullari, S. Ahmadzadeh, G. Kandhola and J. W. Kim, *Compr. Rev. Food Sci. Food Saf.*, 2022, **21**, 4610–4639, DOI: 10.1111/1541-4337.13049.
11 L. Manzocco, K. S. Mikkonen and C. A. García-González, *Food Struct.*, 2021, **28**, 100188, DOI: 10.1016/j.foostr.2021.100188.
12 H. P. S. Abdul Khalil, E. Bashir Yahya, F. Jummaat, A. S. Adnan, N. G. Olaiya, S. Rizal, C. K. Abdullah, D. Pasquini and S. Thomas, *Prog. Mater. Sci.*, 2023, **131**, 101014, DOI: 10.1016/j.pmatsci.2022.101014.
13 S. Kaur, J. Chen and A. Ubeyitogullari, *Sustainable Food Proteins*, 2025, **3**, e70011, DOI: 10.1002/sfp2.70011.
14 S. Ahmadzadeh and A. Ubeyitogullari, *Carbohydr. Polym.*, 2023, **301**, 120296, DOI: 10.1016/j.carbpol.2022.120296.
15 L. T. Possari, P. F. Ávila, M. Brienzo, C. G. Otoni, T. Budtova and S. H. P. Bettini, *ACS Sustainable Resour. Manage.*, 2025, **2**, 944–952, DOI: 10.1021/acssusresmgt.4c00511.

16 S. Karamikamkar, E. P. Yalcintas, R. Haghniaz, N. R. de Barros, M. Mecwan, R. Nasiri, E. Davoodi, F. Nasrollahi, A. Erdem, H. Kang, J. Lee, Y. Zhu, S. Ahadian, V. Jucaud, H. Maleki, M. R. Dokmeci, H. J. Kim and A. Khademhosseini, *Adv. Sci.*, 2023, **10**, e2204681, DOI: 10.1002/advs.202204681.
17 J. Yan, S. Jiang, C. Lin, W. Wang, L. Liu, H. Tang and R. Guo, *Int. J. Biol. Macromol.*, 2025, **322**, 146476, DOI: 10.1016/j.ijbiomac.2025.146476.
18 M. Kloster, M. A. Mosiewicki and N. E. Marcovich, *Int. J. Biol. Macromol.*, 2025, **329**, 147764, DOI: 10.1016/j.ijbiomac.2025.147764.
19 M. He, Y. Huang, Z. Cui, Z. Cheng, W. Cao, G. Wang, W. Yao and M. Feng, *Gels*, 2026, **12**, 76, DOI: 10.3390/gels12010076.
20 M. Jentzsch, V. Albiez, T. C. Kardamakis and T. Speck, *Soft Matter*, 2024, **20**, 2804–2811, DOI: 10.1039/d3sm01511d.
21 H. Kumar, K. Bhardwaj, R. Sharma, E. Nepovimova, K. Kuča, D. S. Dhanjal, R. Verma, P. Bhardwaj, S. Sharma and D. Kumar, *Molecules*, 2020, **25**, 2812, DOI: 10.3390/molecules25122812.
22 N. Sadaf, A. Tuhanioglu, N. Hettiarachchy and A. Ubeyitogullari, *RSC Adv.*, 2024, **14**, 5851–5862, DOI: 10.1039/d3ra07426a.
23 K. Liu, *Algal Res.*, 2019, **40**, 101486, DOI: 10.1016/j.algal.2019.101486.
24 M. D. R. Lenie, S. Ahmadzadeh, F. Van Bockstaele and A. Ubeyitogullari, *Food Hydrocoll.*, 2024, **153**, 109989, DOI: 10.1016/j.foodhyd.2024.109989.
25 F. T. Silva, L. M. Fonseca, G. P. Bruni, R. L. Crizel, E. G. Oliveira, E. d. R. Zavareze and A. R. G. Dias, *Int. J. Biol. Macromol.*, 2023, **249**, 126108, DOI: 10.1016/j.ijbiomac.2023.126108.
26 V. T. Nguyen, L. Q. Ha, T. D. L. Nguyen, P. H. Ly, D. M. Nguyen and D. Hoang, *ACS Omega*, 2021, **7**, 1003–1013, DOI: 10.1021/acsomega.1c05586.
27 Z. Yu, C. Hu, A. B. Dichiara, W. Jiang and J. Gu, *Nanomaterials*, 2020, **10**, 169, DOI: 10.3390/nano10010169.
28 Y. Li, H. Zhao, K. Xiang, D. Li, C. Liu, H. Wang, W. Pang, L. Niu, R. Yu and X. Sun, *J. Food Eng.*, 2024, **365**, 111828, DOI: 10.1016/j.jfoodeng.2023.111828.
29 D. Heaney and O. I. Padilla-Zakour, *Foods*, 2025, **14**, 3267, DOI: 10.3390/foods14183267.
30 S. Mishra, B. Prabhakar, P. S. Kharkar and A. M. Pethe, *ACS Omega*, 2022, **8**, 1140–1145, DOI: 10.1021/acsomega.2c06571.
31 S. Gaind, *Waste Biomass Valoriz.*, 2016, **8**, 1351–1360, DOI: 10.1007/s12649-016-9682-2.
32 J. A. Dávila, M. Rosenberg and C. A. Cardona, *Waste Biomass Valoriz.*, 2015, **6**, 253–261, DOI: 10.1007/s12649-014-9339-y.
33 J. Ángel Siles López, Q. Li and I. P. Thompson, *Crit. Rev. Biotechnol.*, 2010, **30**, 63–69, DOI: 10.3109/07388550903425201.
34 B. Enkhmaa, P. Surampudi, E. Anuurad and L. Berglund, in *Endotext*, ed. K. R. Feingold, S. F. Ahmed, B. Anawalt, M. R. Blackman, A. Boyce, G. Chrousos, E. Corpas, W. W. de Herder, K. Dhatariya, K. Dungan, J. Hofland, S. Kalra, G. Kaltsas, N. Kapoor, C. Koch, P. Kopp, M. Korbonits, C. S. Kovacs, W. Kuohung, B. Laferrère, M. Levy, E. A. McGee, R. McLachlan, R. Muzumdar, J. Purnell, R. Rey, R. Sahay, A. S. Shah, F. Singer, M. A. Sperling, C. A. Stratakis, D. L. Trence and D. P. Wilson, MDText.com, Inc.Copyright © 2000-2025, MDText.com, Inc., South Dartmouth (MA), 2000.
35 K. D. Sharma, S. Karki, N. S. Thakur and S. Attri, *J. Food Sci. Technol.*, 2011, **49**, 22–32, DOI: 10.1007/s13197-011-0310-7.
36 V. Núñez-Gómez, R. González-Barrio, N. Baenas, D. A. Moreno and M. J. Periago, *Int. J. Mol. Sci.*, 2022, **23**, 13309, DOI: 10.3390/ijms232113309.
37 K. Rodkantuk, N. Chiewchan and S. Devahastin, *Int. J. Food Sci. Technol.*, 2021, **56**, 4316–4327, DOI: 10.1111/ijfs.15234.
38 J. Zhang, S. Hu, Y. Ding, R. Huang, Q. Ren, S. Su, Y. Wang, L. Jiang, J. Xu and J. Xiang, *Processes*, 2023, **11**, 892, DOI: 10.3390/pr11030892.
39 S. Khodavandegar, R. Zare and P. Fatehi, *Ind. Crops Prod.*, 2025, **234**, 121540, DOI: 10.1016/j.indcrop.2025.121540.
40 A. López Ortiz, J. Rodríguez Ramírez and L. L. Méndez Lagunas, *Int. J. Food Prop.*, 2013, **16**, 1516–1529, DOI: 10.1080/10942912.2011.599090.
41 A. Asqardokht-Aliabadi, J. Mohammadzadeh Milani and A. Dufresne, *J. Agric. Food Res.*, 2025, **24**, 102331, DOI: 10.1016/j.jafr.2025.102331.
42 O. Korhonen and T. Budtova, *Composites, Part A*, 2020, **137**, 106027, DOI: 10.1016/j.compositesa.2020.106027.
43 X. Yue, T. Zhang, D. Yang, F. Qiu and Z. Li, *J. Clean. Prod.*, 2018, **199**, 411–419, DOI: 10.1016/j.jclepro.2018.07.181.
44 F. Bigi, E. Maurizzi, H. Haghighi, H. Siesler, F. Licciardello and A. Pulvirenti, *Foods*, 2023, **12**, 960, DOI: 10.3390/foods12050960.
45 Y. F. Shih, T. Y. Pan, T. Y. Lu, T. H. Huang and C. W. Chang, *Waste Manag. Bull.*, 2025, **3**, 100258, DOI: 10.1016/j.wmb.2025.100258.
46 X. Li, L. Wang, P. Jiang, Y. Zhu, W. Zhang, R. Li and B. Tan, *LWT-Food Sci. Technol.*, 2023, **173**, 114304, DOI: 10.1016/j.lwt.2022.114304.
47 Z. Wang, H. Huang, Y. Wang, M. Zhou and W. Zhai, *Materials*, 2023, **17**, 172, DOI: 10.3390/ma17010172.
48 A. Dourbash, S. Motahari and H. Omranpour, *J. Non-Cryst. Solids*, 2014, **405**, 135–140, DOI: 10.1016/j.jnoncrysol.2014.09.013.
49 H. Omranpour and S. Motahari, *J. Non-Cryst. Solids*, 2013, **379**, 7–11, DOI: 10.1016/j.jnoncrysol.2013.07.025.
50 S. D. Bhagat, C.-S. Oh, Y.-H. Kim, Y.-S. Ahn and J.-G. Yeo, *Microporous Mesoporous Mater.*, 2007, **100**, 350–355, DOI: 10.1016/j.micromeso.2006.10.026.
51 S. J. Eichhorn and W. W. Sampson, *J. R. Soc. Interface*, 2009, **7**, 641–649, DOI: 10.1098/rsif.2009.0374.
52 H. Fan, B. Xue, J. Lu, T. Sun, Q. Zhao, Y. Liu, M. Niu, S. Yu, Y. Yang and L. Zhang, *Int. J. Biol. Macromol.*, 2025, **291**, 139144, DOI: 10.1016/j.ijbiomac.2024.139144.
53 F. Tomul, Y. Arslan, F. T. Başoğlu, Y. Babuçcuoğlu and H. N. Tran, *J. Environ. Manage.*, 2019, **238**, 296–306, DOI: 10.1016/j.jenvman.2019.02.088.
54 N. Johar, I. Ahmad and A. Dufresne, *Ind. Crops Prod.*, 2012, **37**, 93–99, DOI: 10.1016/j.indcrop.2011.12.016.

55 K. Gao, B. Liu, B. Wu, Y. Guo, C. Song, S. Nan, J. Dai, Y. Shen and H. Ma, *Agriculture*, 2024, **14**, 803, DOI: 10.3390/agriculture14060803.
56 S. Ma, Z. Yang, H. Sun, T. Wu, S. Pan and X. Xu, *Int. J. Biol. Macromol.*, 2025, **330**, 148164, DOI: 10.1016/j.ijbiomac.2025.148164.
57 W. L. Liang, J. S. Liao, J. R. Qi, W. X. Jiang and X. Q. Yang, *Food Chem.*, 2022, **375**, 131806, DOI: 10.1016/j.foodchem.2021.131806.
58 Ș. O. Dima, D. Constantinescu Aruxandei, N. Tritean, M. Ghiurea, L. Capră, C. A. Nicolae, V. Faraon, C. Neamțu and F. Oancea, *Plants*, 2023, **12**, 3016, DOI: 10.3390/plants12163016.
59 L. Chen, H. Zhang and X. Sui, *Int. J. Biol. Macromol.*, 2025, **327**, 147551, DOI: 10.1016/j.ijbiomac.2025.147551.
60 W. Luo, E. Gonzalez, A. Zarei, S. Calleja, B. Rozzi, J. Demieville, H. Li, M.-J. Truco, D. Lavelle, R. Michelmore, J. M. Dyer, M. A. Jenks and D. Pauli, *Heliyon*, 2024, **10**, e27226, DOI: 10.1016/j.heliyon.2024.e27226.
61 J. López Mercado, A. Nambo, M. E. Toribio Nava, O. Melgoza Sevilla, L. Cázarez Barragán, L. Cajero Zul, L. G. Guerrero Ramírez, B. E. Handy and M. G. Cardenas Galindo, *Clean Technol. Environ. Policy*, 2018, **20**, 1413–1422, DOI: 10.1007/s10098-018-1570-y.
62 J. Müller-Maatsch, M. Bencivenni, A. Caligiani, T. Tedeschi, G. Bruggeman, M. Bosch, J. Petrusan, B. Van Droogenbroeck, K. Elst and S. Sforza, *Food Chem.*, 2016, **201**, 37–45, DOI: 10.1016/j.foodchem.2016.01.012.
63 M. Yin, Z. Fu, X. Yu, X. Wang and Y. Lu, *Polymers*, 2025, **17**, 1686, DOI: 10.3390/polym17121686.
64 V. Núñez Gómez, M. Jesús Periago, J. Luis Ordóñez Díaz, G. Pereira Caro, J. Manuel Moreno Rojas and R. González Barrio, *Food Res. Int.*, 2024, **177**, 113718, DOI: 10.1016/j.foodres.2023.113718.
65 S. Wanlapa, K. Wachirasiri, D. Sithisam-ang and T. Suwannatup, *Int. J. Food Prop.*, 2011, **18**, 1306–1316, DOI: 10.1080/10942912.2010.535187.
66 C. Fu, D. Zhan, G. Tian, A. Yu, L. Yao and Z. Guo, *ACS Appl. Mater. Interfaces*, 2024, **16**, 35740–35751, DOI: 10.1021/acsami.4c05041.
67 M. Vera-Mahecha, M. A. Noriega and D. A. Castellanos, *J. Food Eng.*, 2025, **397**, 112605, DOI: 10.1016/j.jfoodeng.2025.112605.
68 U. Michael Igolima, S. J. Abbey, A. O. Ifelebuegu and E. U. Eyo, *Materials*, 2023, **16**, 1092, DOI: 10.3390/ma16031092.
69 Q. Zhou, X. Jiang, Y. Guo, G. Zhang and W. Jiang, *Chemosphere*, 2018, **201**, 519–529, DOI: 10.1016/j.chemosphere.2018.03.045.
70 S. Zhao, Y. Li, M. Wang, B. Chen, Y. Zhang, Y. Sun, K. Chen, Q. Du, X. Pi, Y. Wang, Z. Jing and Y. Jin, *Int. J. Biol. Macromol.*, 2023, **253**, 126458, DOI: 10.1016/j.ijbiomac.2023.126458.
71 B. H. Hameed, *J. Hazard. Mater.*, 2009, **162**, 939–944, DOI: 10.1016/j.jhazmat.2008.05.120.
72 J. B. Adeoye, S. Y. Lau, Y. H. Tan, Y. Y. Tan, T. Chiong, N. M. Mubarak, G. Anbuchezhiyan, M. Khalid and J. T. W. Ng, *Discov. Appl. Sci.*, 2025, **7**, 1285, DOI: 10.1007/s42452-025-07250-4.
73 B. Qiu, Q. Shao, J. Shi, C. Yang and H. Chu, *Sep. Purif. Technol.*, 2022, **300**, 121925, DOI: 10.1016/j.seppur.2022.121925.
74 W. Ji, H. Jin, H. Wang, S. Tabassum, Y. Lou, X. Fan, M. Ren and J. Wang, *Colloids Surf., A*, 2025, **715**, 136615, DOI: 10.1016/j.colsurfa.2025.136615.
75 S. R. Al Mhyawi, N. A. H. Abdel Tawab and R. M. El Nashar, *Polymers*, 2023, **15**, 277, DOI: 10.3390/polym15020277.
76 N. Khumalo, S. Mohomane, V. Elumalai and T. Motaung, *Polymers*, 2025, **17**, 2983, DOI: 10.3390/polym17222983.
77 N. I. I. Zamri, S. L. N. Zulmajdi, N. Z. A. Daud, A. H. Mahadi, E. Kusrini and A. Usman, *SN Appl. Sci.*, 2021, **3**, 222, DOI: 10.1007/s42452-021-04245-9.
78 J. Qiu, P. Fan, Y. Feng, F. Liu, C. Ling and A. Li, *Environ. Pollut.*, 2019, **254**, 113117, DOI: 10.1016/j.envpol.2019.113117.